Comparison of independent evolutionary origins reveals both convergence and divergence in the metabolic mechanisms of symbiosis

Megan E. S. Sørensen[1], A. Jamie Wood[2], Ewan J. A. Minter[1], Chris D. Lowe[3], Duncan D. Cameron[1], Michael A. Brockhurst[1]

1. Department of Animal and Plant Sciences, University of Sheffield, Sheffield S10 2TN, UK

2. Department of Biology, University of York, York YO10 5DD, UK

3. Centre for Ecology and Conservation, University of Exeter, Penryn Campus, Cornwall TR10 9FE, UK

Lead contact Michael Brockhurst (m.brockhurst@sheffield.ac.uk)

Summary

Through the merger of once independent lineages, symbiosis promotes the acquisition of new traits and the exploitation of inaccessible ecological niches [1,2], driving evolutionary innovation and important ecosystem functions [3–6]. The transient nature of establishment makes study of symbiotic origins difficult, but experimental comparison of independent originations could reveal the degree of convergence in the underpinning mechanisms [7,8]. We compared the metabolic mechanisms of two independent origins of the *Paramecium bursaria-Chlorella* photosymbiosis [9–11] using a reciprocal metabolomic pulse-chase method. This showed convergent patterns of nutrient exchange and utilisation for host-derived nitrogen in the *Chlorella* genotypes [12,13] and symbiont-derived carbon in the *P. bursaria* genotypes [14,15]. Consistent with a convergent primary nutrient exchange, partner-switched host-symbiont pairings were functional. Direct competition of hosts containing native or recombined symbionts against isogenic symbiont-free hosts showed that the fitness benefits of symbiosis for hosts increased with irradiance but varied by genotype. Global metabolism varied more between the *Chlorella* than the *P. bursaria* genotypes, and suggested divergent mechanisms of light management. Specifically, the algal symbiont genotypes either produced photo-protective carotenoid pigments at high irradiance or more chlorophyll, resulting in corresponding differences in photosynthetic efficiency and non-photochemical quenching among host-symbiont pairings. These data suggest that the multiple origins of the *P. bursaria-Chlorella* symbiosis use a convergent nutrient exchange, whereas other photosynthetic traits linked to the functioning of the photosymbiosis have diverged. While convergence enables partner-switching among diverse strains,

phenotypic mismatches resulting from divergence of secondary-symbiotic traits could mediate host-symbiont specificity in nature.

Results and Discussion

Independent evolutionary origins of a beneficial symbiotic relationship suggests that a strong selective advantage has, on multiple occasions, overcome the inherent conflict between the self-interest of the partners [16,17]. Independent origins of symbiosis appear to be common and have been reported in diverse symbiotic relationships [18–21]. Experimental comparison of independent origins could reveal the degree of convergence versus divergence in the underpinning mechanisms [7,8]. A convergent nutrient exchange would suggest evolutionary constraint and limited viable routes to symbiosis, but may allow partner-switching between independent lineages, whereas divergence would tend to drive host-symbiont specificity. Here we use the experimentally tractable microbial symbiosis between the heterotrophic ciliate *Paramecium bursaria* and the photosynthetic green alga *Chlorella* sp [9]. These species engage in a facultative photosymbiosis that is widely distributed in freshwater habitats [22], wherein ~100-600 algal cells live inside a ciliate cell and provide products of photosynthesis in exchange for organic nitrogen [14,23]. This symbiotic interaction has originated multiple times and forms two distinct biogeographical clades, specifically, the European clade and the American/Japanese clade [10,11]. Using a representative of each clade [the strain 186b originally isolated in the UK and strain HA1 originally isolated in Japan (Table S1); clade identity was confirmed by diagnostic PCR (Figure S1)] we first tested whether these strains used convergent biochemical mechanisms of carbon (from the photosynthetic endosymbiotic *Chlorella*) for nitrogen (acquired by the protist host though the

ingestion and digestion of free-living bacteria) exchange [14]. To do this, we devised a reciprocal, temporally-resolved, metabolomic pulse chase experiment that simultaneously monitored nitrogen and carbon assimilation in the symbiont and host, respectively. Specifically, using ^{15}N-labelled bacterial necromass, we traced isotopic enrichment derived from N assimilated through *P. bursaria* digestion in *Chlorella* metabolites. In parallel, using ^{13}C-lablled HCO_3 we traced isotopic enrichment derived from C fixed by *Chlorella* photosynthesis in *P. bursaria* metabolites. The quantity of every individual metabolite in each sample was determined using Liquid Chromatography Time of Flight Mass Spectrometry (LC-ToFMS). This allowed the metabolic fate of resources exchanged between symbiotic partners to be quantified over time, allowing comparison of symbiotic metabolism between the strains.

We used Random Forest models, a form of computational learning involving the construction of an extensive array of possible compatible decision trees, to identify which metabolites were associated with isotopic enrichment. Among *Chlorella* metabolites we observed a shared ^{15}N isotopic enrichment response among strains (i.e. high-ranking score in both strains) in 46% of all metabolites (78 % of nitrogen-containing metabolites), suggesting that both *Chlorella* strains directed the exchanged nitrogen through metabolism in similar ways (Figure 1). Similarly, we observed a shared ^{13}C enrichment response in 75 % of *P. bursaria* metabolites (78% of carbon-containing metabolites), suggesting a high degree of convergence between the *P. bursaria* host strains in how they utilised the C derived from their algal symbionts (Figure 1). The pattern of shared enrichment among strains was consistently high for both ^{15}N and ^{13}C isotopic enrichment across all sampled time-points, suggesting a conserved nutrient exchange (Figure 1). Smaller proportions of

metabolites showed an asymmetric response (i.e., were high-ranked in one strain but low-ranked in the other; for ^{15}N enrichment, 20.55% in 186b *Chlorella* and 9.55% in HA1 *Chlorella*; for ^{13}C enrichment 13.17% in 186b *P. bursaria* and 3.42% in HA1 *P. bursaria*), suggesting only limited divergence in utilisation of exchanged metabolites has occurred between these host-symbiont clades.

Co-enriched metabolites with the strongest enrichment over time were identified using LC-ToFMS (simultaneously resolving the monoisotopic mass and chromatographic retention time for each M/Z). For ^{15}N co-enrichment in *Chlorella* (Table S2), we identified metabolites associated with the amino acid and purine pathways, which have both previously been suggested as probable N exchange metabolites in this symbiosis [12,24–27]. Targeted analyses of these pathways were used to calculate the enrichment dynamics in the constituent metabolites. These dynamics indicated that an amino acid is the more likely N exchange metabolite from *P. bursaria* to *Chlorella* in both clades. Although our first sampling time-point was not early enough to permit direct observation of metabolite exchange itself, downstream enrichment profiles suggest that the most likely candidate exchange metabolite is arginine (see Figure S4), an amino acid known to support growth of *Chlorella* as its sole N source [28]. In addition, we observed co-enrichment in larger, N-rich metabolites, including chlorophyll precursors, which most likely represent the largest N-sinks for *Chlorella*, thus becoming enriched in ^{15}N as a function of N demand. For ^{13}C enrichment in *P. bursaria* (Table S3), we identified metabolites involved in carbohydrate and lipid metabolism, suggesting that symbiont derived C was directed to carbon storage, as well as enrichment in central and amino acid metabolism, which are likely to have a high turnover of carbon and represent strong carbon sinks.

For some carbohydrate storage metabolites, we observed stronger differences in ^{13}C enrichment between light conditions in the 186b compared to the HA1 strain (Figure S3), indicating strain differences in the rate of flux through some of co-enriched pathways.

The pulse-chase analysis suggests that these *P. bursaria-Chlorella* strains, representing independent origins of the symbiosis, show convergent utilisation of partner-derived nutrients, and we hypothesised therefore that partner-switched host-symbiont pairings would be functional. To test this, we performed a reciprocal cross-infection experiment whereby the *P. bursaria* host strains were cured of their native algal symbiont, and subsequently re-infected with either their native algal symbiont or the reciprocal non-native algal symbiont. We then directly competed each host-symbiont pairing against its respective symbiont-free host strain across a light gradient. Note that reinfection of aposymbiotic host populations by symbionts occurs over far longer timescales (i.e. several weeks) than the competition assay, such that this process is unlikely to affect relative fitness estimates. We used flow cytometry to quantify the proportion of green (with symbiont) versus white (symbiont-free) host cells at the start and end of the growth cycle to calculate the selection rate [23], thus providing a direct measure of the fitness effect of symbiosis for hosts. All the symbiont pairings showed a classic photosymbiotic reaction norm, such that the relative fitness of hosts with symbionts versus hosts without symbionts increased with increasing irradiance (Figure 2), and more steeply in the HA1 host background (host genotype * light environment interaction, ANOVA, $F_{3,31} = 29.34$, $P < 0.001$). This confirms that both host genotypes could derive the benefits of symbiosis from either

of the symbiont genotypes, but that the fitness effect of symbiosis varied between strains.

These light-dependent differences in the fitness of the host-symbiont pairings suggest that the HA1 and 186b strains may have diverged in aspects of their metabolism and physiology besides the primary symbiotic nutrient exchange. To characterise potential differences in global metabolism between the HA1 and 186b host-symbiont strains, we performed untargeted metabolomics analyses on the unlabelled metabolites from the separated *Chlorella* and *P. bursaria* fractions of both the native host-symbiont pairings. We observed a range of metabolites that differentiated the 186b and HA1 *Chlorella* strains (Table S4), and metabolism differed more between strains than it did between light conditions within strains (Figure 3). Notably, the HA1 *Chlorella* strain displayed higher levels of several carotenoids than the 186b *Chlorella* strain, particularly at high irradiance, whereas the 186b *Chlorella* strain displayed higher levels of metabolites involved in chlorophyll and ubiquinol metabolism than the HA1 *Chlorella* strain at both low and high irradiance (Figure 4). Fewer metabolites distinguished the global metabolism of the *P. bursaria* strains (Table S4). In all cases these metabolites were present at higher levels in the 186b *P. bursaria* strain compared to the HA1 *P. bursaria* strain (Figure S2), and neither strain's metabolism varied significantly with irradiance (Figure S2). The identified metabolites that distinguished the strains were associated with a range of functions, including amino acid metabolism, amino sugars, and sphingolipid metabolism. Several other metabolites, although present in the host fraction, are likely to have been secreted into the host cytoplasm by the algal symbiont or be derived from the bacterial necromass. These include a zeatin

candidate, which may play a role in *Chlorella* signalling, and several metabolites identified as putative antibiotics.

The clear differences in global metabolism between the algal strains suggests that they may vary in their photophysiology. To test this, we measured several key photochemical parameters in the native and partner-switched host-symbiont pairings acclimated to a range of light levels. For two measures of photosynthetic efficiency — Fv/Fm (the intrinsic efficiency of photosystem II [PSII], Figure 5a) and Φ_{PSII} (the proportion of the light absorbed by chlorophyll associated with PSII that is used in photochemistry, Figure 5b) [29] — we observed a significant host genotype by symbiont genotype by light environment interaction (for F_vF_m ANOVA, $F_{7,232} = 86.41$, $P<0.001$; for Φ_{PSII} nlme model intercept summary ANOVA, $F_{11,24} = 11.66$, $P<0.001$ (see Data S1 for full statistical output)). In the HA1 *P. bursaria* host, the pattern of photosynthetic efficiency across the light gradient did not vary with algal strain, whereas in the 186b *P. bursaria* host, the native 186b *Chlorella* showed lower photosynthetic efficiency than the HA1 *Chlorella* at low growth irradiance, but the pattern was reversed at high growth irradiance. These patterns are consistent with the observed differences in carotenoid metabolism among the *Chlorella* strains: The HA1 *Chlorella* produced more carotenoids at high irradiance than the 186b *Chlorella*, and carotenoids perform a role in photoprotection and can therefore decrease the light energy that reaches the photosystems and thereby limit photosynthesis.

Non-photochemical quenching is used by photosynthetic organisms to safely deal with excess and potentially damaging light energy and was estimated using the normalised Stern-Volmer coefficient (NSV). The intercept of the NSV response

(Figure 5c) across the actinic light gradient was significantly affected by host genotype, suggesting differences among the host genotypes in their ability to photo-protect algal symbionts (ANOVA, $F_{1,34} = 4.74$, $P<0.05$). Meanwhile, both symbiont genotype and growth irradiance affected the first coefficient (ANOVA, $F_{3,32} = 5.56$, $P<0.01$); and symbiont genotype affected the second coefficient (ANOVA, $F_{1,34} = 8.932$, $P<0.01$) (see Data S1 for full statistical output). Higher levels of NSV and steeper NSV reaction norms for the 186b *Chlorella*, particularly in its native host background, are consistent with the greater investment in photosynthetic machinery observed in the metabolome, allowing this genotype to better dissipate excess light energy as heat whilst not compromising photosynthetic efficiency.

Mixotrophic photosymbioses are common and play a vital role in biogeochemical cycling in terrestrial and aquatic ecosystems [30–32]. Their breakdown, often driven by environmental change, can be rescued by partner-switching to restore symbiotic function [33,34]. Our findings suggest that convergence among independent symbiotic origins upon a shared primary symbiotic nutrient exchange enables partner-switching between genetically divergent clades. This stands in contrast to the diversity of exchange metabolites used in photosymbioses more broadly. For example, just amongst photosymbiotic cnidaria (i.e. corals, anemones, jellyfish) organic carbon transfer from symbiont to host occurs in the form of glycerol, glucose, maltose, and a variety of lipids and amino acids [35]. Thus, while a variety of potential metabolic solutions to the photosymbiotic nutrient exchange exist, perhaps explaining the abundance and diversity of photosymbioses, within specific symbiotic interactions the optimal solution may be more constrained, resulting in evolutionary convergence among independent originations. The concurrent divergence in algal

photophysiology allowed hosts, through partner-switching, to acquire symbionts with different properties, potentially enabling adaptation to new environments. Crucially, symbiont replacement providing hosts with new adaptive traits is critical in natural populations responding to environmental change; for example, reinfection of corals by thermally tolerant symbionts enables recovery following thermal bleaching events [36–38]. Finally, we observed differences among the *P. bursaria-Chlorella* clades in their division of labour between host and symbiont contributions to photoprotection. This may be a common feature of photosymbioses [39,40], for example some pelagic zooplankton and jellyfish hosts adopt behavioural strategies to photoprotect algal symbionts [41], and could be a key mechanism of host-symbiont specificity by mediating genotype by genotype by environment interactions. Host-symbiont specificity and partner-switching are common features of many symbioses [42–46] suggesting that our findings are likely to be of wider relevance beyond photosymbioses. Multiple independent evolutionary origins have occurred in diverse symbiotic relationships [18–21]. While this suggests a strong selective imperative for these symbioses, it may also provide important adaptive potential through functional divergence among originations enabling their resilience to environmental change.

Acknowledgements

This work was funded by grant NE/K011774/2 from the Natural Environment Research Council, UK to MAB, CDL, DDC, and AJW, and a White Rose DTP studentship from the Biotechnology and Biological Sciences Research Council, UK to MESS (BB/M011151/1). The funders had no role in the design of the study, the

collection, analysis and interpretation of data, or the writing of the manuscript. We are grateful to Heather Walker for assistance.

Author contributions

MB, DC, MS, EM, CL conceived and designed the study. MS and EM conducted experimental work. MS, CL and DC analysed the data. MS and MB drafted the manuscript. All authors commented on the manuscript.

Conflict of interest

The authors declare that they have no conflicting interests.

Figure Legends

Figure 1: Correlated metabolite enrichment for the 186b and HA1 *Paramecium bursaria* and *Chlorella* strains over time.

Each data point represents a metabolite and the scatterplot displays the Random Forest rank order of each metabolite in both strains. The rank order value is positively correlated with magnitude of the enrichment signal. A,C,E,G.) N^{15} enrichment in the *Chlorella* fraction. B,D,F,H.) C^{13} enrichment in the *P. bursaria* fraction. For all panels, responses are presented as the mean (n=500), for further details regarding the Random Forest models see the methods section.

Figure 2: **Fitness of the native and non-native host-symbiont pairings relative to isogenic symbiont-free hosts**.

Selection rate measurements were calculated from the change in proportion between the symbiotic and symbiont-free *Paramecium* over the course of the experiment. The line of selection rate = 0 represents when the two competed populations have equal fitness (e.g. when the symbiotic *P. bursaria* have equal fitness to the symbiont-free *P. bursaria*). Presented as the mean (n=3) ±SE.

Figure 3: **Differences in *Chlorella* global metabolism between strains across light conditions.**

Represented as volcano plots with the fold change of each metabolite against its statistical significance. The data points are highlighted at two false discovery rate (FDR) values, and if the Log_2(fold change) is greater than 1 or less than -1. A.) Comparing the expression between the two strains within the high light condition. B.)

Comparing the expression between the two strains within the low light condition. C.) Comparing expression between the two light levels within the HA1 strain. D.) Comparing expression between the two light levels within the 186b strain. See Figure S2 for the equivalent plot for the *P. bursaria* metabolite comparisons.

Figure 4: **Metabolites associated with the differential light responses of the 186b and HA1 *Chlorella* strains.**

The metabolites presented were highlighted by the volcano plot analysis and represent the divergent strategies in light management between the two strains. The relative abundance of the metabolites is plotted within the two strains at the two light conditions. The top three panels (A-C) show metabolites that have been identified as carotenoids and the lower three panels (D-F) show metabolites that have been identified as either chlorophyll or ubiquinone compounds. For all panels, responses are presented as the mean (n=12) ±SE.

Figure 5: **Photophysiology measurements for the native and non-native host-symbiont pairings**.

A) Estimates of the maximum quantum yield of photosystem II (F_v/F_m) across growth irradiances. B) Light-adapted quantum yield of photosystem II (Φ_{PSII}) across growth irradiances, lines represent exponential decay models using nlme package in R. C.) The normalised Stern-Volmer quenching coefficient (NSV = F_o'/F_v') across growth irradiances, presented at polynomial models. For all panels, responses are presented as the mean (n=3) ±SE. See Data S1 for model details.

STAR Methods

LEAD CONTACT AND MATERIALS AVAILABILITY

Further information and requests for resources and reagents should be directed to and will be fulfilled by the Lead Contact, Michael Brockhurst (m.brockhurst@sheffield.ac.uk). These resources and reagents will be made available upon request.

EXPERIMENTAL MODEL AND SUBJECT DETAILS

Symbiotic *Paramecium bursaria* stock cultures were maintained at 25^{o}c under a 14:10 L:D cycle with 50 μE m^{-2} s^{-1} of light. Grown in bacterized Protozoan Pellet Media (PPM, Carolina Biological Supply), made to a concentration of 0.66 g L^{-1} with Volvic natural mineral water, and inoculated approximately 20 hours prior to use with *Serratia marscesens* from frozen glycerol stocks. The two natural strains used were: 186b (CCAP 1660/18) obtained from the Culture Collection for Algae and Protozoa (Oban, Scotland), and HA1 isolated in Japan and obtained from the Paramecium National Bio-Resource Project (Yamaguchi, Japan).

To isolate *Chlorella* from the symbiosis, symbiotic cultures were first washed and concentrated with a 11μm nylon mesh using sterile Volvic. The suspension was then ultra-sonicated using a Fisherbrand™ Q500 Sonicator (Fisher Scientific, NH, USA), at a power setting of 20% for 10 seconds sonification to disrupt the host cells. The liquid was then spotted onto Bold Basal Media plates (BBM) [47], from which green colonies were streaked out and isolated over several weeks. Plate stocks were maintained by streaking out one colony to a fresh plate every 3/4 weeks.

Symbiont-free *P. bursaria* were made by treating symbiotic cultures with paraquat (10 µg mL^{-1}) for 3 to 7 days in high light conditions (>50 µE m^{-2} s^{-1}), until the host cells were visibly symbiont free. The cultures were then extensively washing with Volvic and closely monitored with microscopy to check that re-greening by *Chlorella* did not occur. Stock cultures of the symbiont-free cells were maintained by batch culture at 25°c under a 14:10 L:D cycle with 3 µE m^{-2} s^{-1} of light and were given fresh PPM weekly.

METHOD DETAILS

Cross Infections

Symbiont-free populations of the two *P. bursaria* strains were re-infected by adding a colony of *Chlorella* from the plate stocks derived from the appropriate strain. The re-greening process was followed by microscopy and took between 2-6 weeks. Over the process, cells were grown at the intermediate light level of 12 µE m^{-2} s^{-1} and were given bacterized PPM weekly.

Diagnostic PCR

The correct algae genotype was confirmed using diagnostic PCR. The *Chlorella* DNA was extracted by isolating the *Chlorella* and then using a standard 6% Chelex100 resin (Bio-Rad) extraction method. ISSR primer '65' were established for *Chlorella vulgaris* by Shen (2008), and was used as described therein. Standard PCR reactions were performed using Go Taq Green Master Mix (Promega) and 0.5µmol L^{-1} of primer. The thermocycler programme was set to: 94°c for 5min, 40 cycles of (94°c for 20sec, 55°c for 1 min, 72°c for 20sec), and 6 min at 72°c.

Fitness assay

P. bursaria cultures, both the symbiotic cross-infections and symbiont-free cells, were washed with Volvic and resuspended in bacterized PPM. The cultures were then split and acclimated at their treatment light level (0,12,50 μE m^{-2} s^{-1}) for five days. Cell densities were counted by fixing 360 μL of each cell culture, in triplicate, in 1% v/v glutaraldehyde in 96-well flat bottomed micro-well plates. Images were taken with a plate reader (Tecan Spark 10M) and cell counts were made using an automated image analysis macro in ImageJ v1.50i [49]. The competitions were started with the target values of 20 green cells and 20 white cells per ml. Cells were sampled on day 0 and day 7 and the proportion of green to white cells was measured using flow cytometry analysis. Green versus white cells were distinguished using single cell fluorescence estimated using a CytoFLEX S flow cytometer (Beckman Coulter Inc., CA, USA) by measuring the intensity of chlorophyll fluorescence (excitation 488nm, emission 690/50nm) and gating cell size using forward side scatter [23]. The measurements were calibrated against 8-peak rainbow calibration particles (BioLegend), and then presented as relative fluorescence to reduce variation across sampling sessions.

Fluorimetry

The cells were washed and concentrated with a 11μm nylon mesh using sterile Volvic and re-suspended in bacterized PPM. The cultures were then split and acclimated to their treatment light condition (12, 24 & 50 μE m^{-2} s^{-1}) for five days. F_v/F_m, Φ_{PSII}, and NSV values were measured by fast repetition rate fluorimetry (FastPro8, Chelsea instruments fluorometer [50] following the manufactures procedure. Cultures were dark acclimated for 15 minutes prior to measurements. For

maximum quantum yield, measurements were repeated until F_v/F_m stabilized (typically 3-5minutes) and F_v/F_m then estimated as an average of 10 measurements. Φ_{PSII} was measured in response to an actinic light source at sequentially increasing irradiances between 0 – 2908 PFD following standard green algae protocol. Peak emission wavelengths of the LED used for excitations was 450nm. Non-photochemical quenching was estimated by the normalised Stern-Volmer coefficient, defined as NSV = F_o'/F_v' [51] and corrects for differences in F_v/F_m between samples.

Metabolomics

Cultures were washed and concentrated with a 11µm nylon mesh using Volvic and re-suspended in bacterized PPM. The cultures were first grown for three days at 50 µE m^{-2} s^{-1} to increase cell densities, and then split and acclimated at their treatment light condition (6 & 50 µE m^{-2} s^{-1}) for three days. For the sampling, the cultures were split into 3 treatment: the control, N^{15} enrichment by the addition of labelled *Serratia marscesens* (100µl per microcosm), or C^{13} enrichment by the addition of $HC^{13}O_3$ (100 mg L^{-1}). The cultures were sampled at four time points (0,2,6,8 hrs after the enrichment event). There were three biological replicates for each sampling event.

At each sampling event, the symbiotic partners were separated in order to a get *P. bursaria* and *Chlorella* metabolic fraction. The *P. bursaria* cells were concentrated with a 11µm nylon mesh using Volvic and then the *P. bursaria* cells were disrupted by sonication (20% power for 10 secs). 1ml of the lysate was pushed through a 1.6µm filter, which caught the intact *Chlorella* cells, and the run-through was collected and stored as the *P. bursaria* fraction. The 1.6µm filter was washed with

5ml cold deionized water, and then reversed so that the *Chlorella* cells were resuspended in 1ml of cold methanol, which was stored as the *Chlorella* fraction.

The samples were analysed with a Synapt G2-Si with Acquity UPLC, recording in positive mode over a large untargeted mass range (50 – 1000 Da). A 2.1x50mm Acuity UPLC BEH C18 column was used with acetonitrile as the solvent. The machine settings are listed in detail below:

Mass spectrometry settings:

Polarity:	positive
Capillary voltage:	2.3 kV
Sample Cone voltage:	20 V
Source Temperature:	100^{o}c
Desolvation temperature:	280^{o}c
Gas Flow:	600 L hr^{-1}
Injected volume:	5µl

Gradient information:

Time (mins)	**Water (%)**	**Acetonitrile (%)**
0	95	5
3	65	35
6	0	100
7.5	0	100
7.6	95	5

The *P. bursaria* and *Chlorella* fraction were analysed separately. The xcms R package [52–54] was used for automatic peak detection by extracting the spectra

415 from the CDF data files, using a step argument of 0.01 m/z. The automatically
416 identified peaks were grouped across samples and were used to identify and correct
417 correlated drifts in retention time from run to run. Pareto scaling was applied to the
418 resulting intensity matrix.
419
420 *Isotope analysis*
421 For the *P. bursaria* isotope analysis the C^{13} labelled samples were compared with
422 the control, while for the *Chlorella* analysis the N^{15} labelled samples were compared
423 to the control. In order to identify isotopic enrichment without user bias, we used
424 Random Forest (RF) models to identify metabolites that associated with the isotope
425 labelling. This is a machine-learning decision-tree based approach that produces
426 powerful multivariate regression and is an established method for high-throughput
427 biological data [55], including metabolomics [56]. The isotope label was used as the
428 response variable to regress against the metabolic profile of each sample. Each
429 random forest model was run with 1000 iterations, and each RF analysis was run
430 500 times to account for uncertainty in the rank score. For each run, the rank score
431 of the RF importance (measured as the mean decrease in Gini) was recorded for
432 each m/z bin. The mean and standard error of the rank score was then calculated to
433 assess the consistency of the variable importance. In total 4 RF models were
434 analysed within each fraction, 1 per timepoint.
435
436 The rank score values were then compared between the strains. The high proportion
437 of shared metabolites were selected and filtered to select those that had a higher
438 relative abundance in the labelled fraction than in the control. From these, the profile
439 of each candidate metabolite was manually checked for isotopic enrichment, and

440 when a clear enrichment profile was present the monoisotopic mass was identified.
441 The enrichment proportion of the isotopic masses to the monoisotopic mass was
442 calculated, and the natural enrichment value within the control fraction was
443 subtracted from the enrichment in the labelled fraction. Following this calculation, it
444 was possible to determine if enrichment had occurred, and if so, the monoisotopic
445 mass was considered a 'mass of interest'.
446
447 *Target Pathway analysis*
448 Given that the low molecular weight compounds in the results of the ^{15}N co-
449 enrichment in *Chlorella* (Table S2) were almost exclusively amino acid or purine
450 related, we focused on these pathways for a further targeted approach. Key
451 compounds of these pathways were selected and searched for in the metabolite
452 dataset. To follow the flow of enriched nitrogen in these pathways, the relative
453 enrichment profile of these compounds compared to the control fraction was
454 calculated. The results were visualised as heatmaps, with the heatmap.2() function
455 from the gplot package [57], based on the method used by Austen et al. (In Press).
456
457 Some of the amino acid metabolism results are plotted in Figure S4 and show that
458 the nitrogen enrichment is focused downstream from arginine. Other aspects of
459 amino acid metabolism, such as that centred around aspartate, serine or lysine,
460 showed little and inconsistent enrichment. Within purine metabolism, the nitrogen
461 enrichment occurred both up and downstream of the purine bases. The enrichment
462 upstream of the purine bases indicates that enriched nitrogen is entering this
463 pathway from the amino acid of central metabolism. Based on this pattern, we

464 believe that the purine pathway is a site of secondary enrichment and it reveals that
465 purine-derivatives present a substantial nitrogen demand.
466
467 Unfortunately, we could not identify a candidate compound for arginine to test if it
468 had the enrichment profile of a transfer molecule (predicted to be a very high initial
469 enrichment that then substantially decreased over time). Such a pattern was not
470 seen for any compound, we suggest, therefore, that our first timepoint was not early
471 enough to capture the initial enrichment events involving the transfer compound
472 itself.
473
474 *Unlabelled analysis*
475 For the unlabelled, control fraction, the data was compared between the strains by
476 calculating the log2(Fold Change) between the conditions (either between the strains
477 within each light level, or between the light levels within each strain) in a series of
478 pair-wise contrasts for each metabolite. Student T-tests were performed between the
479 relative abundances of the paired comparisons. The *Benjamini–Hochberg* procedure
480 was used to account for the high number of multiple P-value comparisons, with the
481 false discovery rate set to 0.1 and 0.05 [58] as highlighted in the volcano plots.
482
483 *Identification of significant masses*
484 Masses of interest were investigated using the MarVis-Suite 2.0 software
485 (http://marvis.gobics.de/) [59], using retention time and mass to compare against
486 KEGG (https://www.genome.jp/kegg/) [60,61] and MetaCyc (https://biocyc.org/) [62]
487 databases. The Metabolomics Standards Initiative requires two independent

488 measures to confirm identity, which the combination of retention time and accurate
489 mass achieves. This analysis therefore confirms level 1 identification.
490
491
492 QUANTIFICATION AND STATISTICAL ANALYSIS
493 Statistical analyses were performed in R v.3.5.0 [63] and all plots were produced
494 using package ggplot2 [64]. Physiology tests were analysed by both ANOVA and
495 ANCOVA, with light, host and symbiont identity as factors. Φ_{PSII} results were
496 analysed with non-linear mixed effects models (nlme) with the nlme R package [65].
497 The Φ_{PSII} data was fitted to an exponential decay function:
498
499 $$\Phi_{PSII} = a e^{(bl)}$$
500 Where *a* is a normalisation constant and *b* is the rate constant. The nlme model
501 included random effects by replicate on each parameter and fixed factors of host,
502 symbiont and light factors that interacted with *a* following model reduction. See the
503 full statistics table (Data S1) for further details on the statistics used.
504
505 DATA AND CODE AVAILABILITY
506 The data has been deposited within Mendeley Data (DOI: 10.17632/6zspctmwpj.1).
507
508
509

Legends for supplementary datasets

Data S1. Statistical outputs for analyses associated with the figures of the main manuscript. Related to Figure 2 and 5

References:

1. Wernegreen, J.J. (2012). Endosymbiosis. Current Biology *22*, R555–R561.

2. Sudakaran, S., Kost, C., and Kaltenpoth, M. (2017). Symbiont Acquisition and Replacement as a Source of Ecological Innovation. Trends in Microbiology *25*, 375–390.

3. Kiers, E.T., and West, S.A. (2015). Evolving new organisms via symbiosis. Science *348*, 392–394.

4. Powell, J.R., and Rillig, M.C. (2018). Biodiversity of arbuscular mycorrhizal fungi and ecosystem function. New Phytol.

5. Baker, A.C. (2003). Flexibility and Specificity in Coral-Algal Symbiosis: Diversity, Ecology, and Biogeography of Symbiodinium. Annual Review of Ecology, Evolution, and Systematics *34*, 661–689.

6. Zook, D.P. (2002). Prioritizing Symbiosis to Sustain Biodiversity: Are Symbionts Keystone Species? In Symbiosis: Mechanisms and Model Systems Cellular Origin, Life in Extreme Habitats and Astrobiology., J. Seckbach, ed. (Dordrecht: Springer Netherlands), pp. 3–12.

7. Sachs, J.L., Skophammer, R.G., and Regus, J.U. (2011). Evolutionary transitions in bacterial symbiosis. PNAS *108*, 10800–10807.

8. Moran, N.A., and Wernegreen, J.J. (2000). Lifestyle evolution in symbiotic bacteria: insights from genomics. Trends in Ecology & Evolution *15*, 321–326.

9. Fujishima, M., and Kodama, Y. (2012). Endosymbionts in Paramecium. European Journal of Protistology *48*, 124–137.

10. Hoshina, R., and Imamura, N. (2008). Multiple Origins of the Symbioses in Paramecium bursaria. Protist *159*, 53–63.

11. Summerer, M., Sonntag, B., and Sommaruga, R. (2008). Ciliate-Symbiont Specificity of Freshwater Endosymbiotic Chlorella (trebouxiophyceae, Chlorophyta)1. Journal of Phycology *44*, 77–84.

12. Kato, Y., Ueno, S., and Imamura, N. (2006). Studies on the nitrogen utilization of endosymbiotic algae isolated from Japanese Paramecium bursaria. Plant Science *170*, 481–486.

13. Kessler, E., and Huss, V. a. R. (1990). Biochemical Taxonomy of Symbiotic Chlorella Strains from Paramecium and Acanthocystis*. Botanica Acta *103*, 140–142.

14. Johnson, M.D. (2011). The acquisition of phototrophy: adaptive strategies of hosting endosymbionts and organelles. Photosynth Res *107*, 117–132.

15. Ziesenisz, E., Reisser, W., and Wiessner, W. (1981). Evidence of de novo synthesis of maltose excreted by the endosymbiotic Chlorella from Paramecium bursaria. Planta *153*, 481–485.

16. Sachs, J.L., and Simms, E.L. (2006). Pathways to mutualism breakdown. Trends in Ecology & Evolution *21*, 585–592.

17. Herre, E.A., Knowlton, N., Mueller, U.G., and Rehner, S.A. (1999). The evolution of mutualisms: exploring the paths between conflict and cooperation. Trends in Ecology & Evolution *14*, 49–53.

18. Muggia, L., Nelson, P., Wheeler, T., Yakovchenko, L.S., Tønsberg, T., and Spribille, T. (2011). Convergent evolution of a symbiotic duet: The case of the lichen genus Polychidium (Peltigerales, Ascomycota). American Journal of Botany *98*, 1647–1656.

19. Masson-Boivin, C., Giraud, E., Perret, X., and Batut, J. (2009). Establishing nitrogen-fixing symbiosis with legumes: how many rhizobium recipes? Trends in Microbiology *17*, 458–466.

20. Boscaro, V., Husnik, F., Vannini, C., and Keeling, P.J. (2019). Symbionts of the ciliate Euplotes: diversity, patterns and potential as models for bacteria–eukaryote endosymbioses. Proceedings of the Royal Society B: Biological Sciences *286*, 20190693.

21. Hulcr, J., and Stelinski, L.L. (2017). The Ambrosia Symbiosis: From Evolutionary Ecology to Practical Management. Annual Review of Entomology *62*, 285–303.

22. Zagata, P., Greczek-Stachura, M., Tarcz, S., and Rautian, M. (2016). The Evolutionary Relationships between Endosymbiotic Green Algae of Paramecium bursaria Syngens Originating from Different Geographical Locations. Folia Biologica *64*, 47–54.

23. Kadono, T., Kawano, T., Hosoya, H., and Kosaka, T. (2004). Flow cytometric studies of the host-regulated cell cycle in algae symbiotic with green paramecium. Protoplasma *223*, 133–141.

24. Soldo, A.T., Godoy, G.A., and Larin, F. (1978). Purine-Excretory Nature of Refractile Bodies in the Marine Ciliate Parauronema acutum*. The Journal of Protozoology *25*, 416–418.

25. Shah, N., and Syrett, P.J. (1984). The uptake of guanine and hypoxanthine by marine microalgae. Journal of the Marine Biological Association of the United Kingdom *64*, 545–556.

26. Quispe, C.F., Sonderman, O., Khasin, M., Riekhof, W.R., Van Etten, J.L., and Nickerson, K.W. (2016). Comparative genomics, transcriptomics, and physiology distinguish symbiotic from free-living Chlorella strains. Algal Research *18*, 332–340.

27. Minaeva, E., and Ermilova, E. (2017). Responses triggered in chloroplast of Chlorella variabilis NC64A by long-term association with Paramecium bursaria. Protoplasma, 1–8.

28. Arnow, P., Oleson, J.J., and Williams, J.H. (1953). The Effect of Arginine on the Nutrition of Chlorella vulgaris. American Journal of Botany *40*, 100–104.

29. Maxwell, K., and Johnson, G.N. (2000). Chlorophyll fluorescence—a practical guide. J Exp Bot *51*, 659–668.

30. Esteban, G.F., Fenchel, T., and Finlay, B.J. (2010). Mixotrophy in Ciliates. Protist *161*, 621–641.

31. Stanley, G.D., and Lipps, J.H. (2011). Photosymbiosis: The Driving Force for Reef Success and Failure. The Paleontological Society Papers *17*, 33–59.

32. Caron, D.A. (2016). Mixotrophy stirs up our understanding of marine food webs. PNAS *113*, 2806–2808.

33. Boulotte, N.M., Dalton, S.J., Carroll, A.G., Harrison, P.L., Putnam, H.M., Peplow, L.M., and van Oppen, M.J. (2016). Exploring the *Symbiodinium* rare biosphere provides evidence for symbiont switching in reef-building corals. The ISME Journal *10*, 2693–2701.

34. Lefèvre, C., Charles, H., Vallier, A., Delobel, B., Farrell, B., and Heddi, A. (2004). Endosymbiont Phylogenesis in the Dryophthoridae Weevils: Evidence for Bacterial Replacement. Mol Biol Evol *21*, 965–973.

35. Yellowlees, D., Rees, T.A.V., and Leggat, W. (2008). Metabolic interactions between algal symbionts and invertebrate hosts. Plant, Cell & Environment *31*, 679–694.

36. Berkelmans, R., and van Oppen, M.J.H. (2006). The role of zooxanthellae in the thermal tolerance of corals: a 'nugget of hope' for coral reefs in an era of climate change. Proceedings of the Royal Society B: Biological Sciences *273*, 2305–2312.

37. Rowan, R. (2004). Thermal adaptation in reef coral symbionts. Nature *430*, 742–742.

38. Kinzie, R.A., Takayama, M., Santos, S.R., and Coffroth, M.A. (2001). The Adaptive Bleaching Hypothesis: Experimental Tests of Critical Assumptions. The Biological Bulletin *200*, 51–58.

39. Ye, S., Bhattacharjee, M., and Siemann, E. (2019). Thermal Tolerance in Green Hydra: Identifying the Roles of Algal Endosymbionts and Hosts in a Freshwater Holobiont Under Stress. Microb Ecol *77*, 537–545.

40. Venn, A.A., Loram, J.E., and Douglas, A.E. (2008). Photosynthetic symbioses in animals. J Exp Bot *59*, 1069–1080.

41. Cimino, M.A., Patris, S., Ucharm, G., Bell, L.J., and Terrill, E. (2018). Jellyfish distribution and abundance in relation to the physical habitat of Jellyfish Lake, Palau. Journal of Tropical Ecology *34*, 17–31.

42. Husnik, F., and McCutcheon, J.P. (2016). Repeated replacement of an intrabacterial symbiont in the tripartite nested mealybug symbiosis. PNAS *113*, E5416–E5424.

43. Koga, R., and Moran, N.A. (2014). Swapping symbionts in spittlebugs: evolutionary replacement of a reduced genome symbiont. The ISME Journal *8*, 1237–1246.

44. Matsuura, Y., Moriyama, M., Łukasik, P., Vanderpool, D., Tanahashi, M., Meng, X.-Y., McCutcheon, J.P., and Fukatsu, T. (2018). Recurrent symbiont recruitment from fungal parasites in cicadas. PNAS *115*, E5970–E5979.

45. Sepp, S.-K., Davison, J., Jairus, T., Vasar, M., Moora, M., Zobel, M., and Öpik, M. (2019). Non-random association patterns in a plant–mycorrhizal fungal network reveal host–symbiont specificity. Molecular Ecology *28*, 365–378.

46. Parker, B.J., Hrček, J., McLean, A.H.C., and Godfray, H.C.J. (2017). Genotype specificity among hosts, pathogens, and beneficial microbes influences the strength of symbiont-mediated protection. Evolution *71*, 1222–1231.

47. Stein, J.R. (1979). (ED.) Handbook of Phycological Methods: Culture Methods and Growth Measurements (Cambridge University Press).

48. Shen, S. (2008). Genetic diversity analysis with ISSR PCR on green algae <Emphasis Type="Italic">Chlorella vulgaris</Emphasis> and <Emphasis Type="Italic">Chlorella pyrenoidosa</Emphasis>. Chin. J. Ocean. Limnol. *26*, 380–384.

49. Schneider, C.A., Rasband, W.S., and Eliceiri, K.W. (2012). NIH Image to ImageJ: 25 years of image analysis. Nature Methods.

50. Oxborough, K., Moore, C.M., Suggett, D.J., Lawson, T., Chan, H.G., and Geider, R.J. (2012). Direct estimation of functional PSII reaction center concentration and PSII electron flux on a volume basis: a new approach to the analysis of Fast Repetition Rate fluorometry (FRRf) data. Limnology and Oceanography: Methods *10*, 142–154.

51. McKew, B.A., Davey, P., Finch, S.J., Hopkins, J., Lefebvre, S.C., Metodiev, M.V., Oxborough, K., Raines, C.A., Lawson, T., and Geider, R.J. (2013). The trade-off between the light-harvesting and photoprotective functions of fucoxanthin-chlorophyll proteins dominates light acclimation in Emiliania huxleyi (clone CCMP 1516). New Phytologist *200*, 74–85.

52. Benton, H.P., Want, E.J., and Ebbels, T.M.D. (2010). Correction of mass calibration gaps in liquid chromatography-mass spectrometry metabolomics data. Bioinformatics *26*, 2488–2489.

53. Smith, C.A., Want, E.J., O'Maille, G., Abagyan, R., and Siuzdak, G. (2006). XCMS: Processing Mass Spectrometry Data for Metabolite Profiling Using Nonlinear Peak Alignment, Matching, and Identification. Anal. Chem. *78*, 779–787.

54. Tautenhahn, R., Böttcher, C., and Neumann, S. (2008). Highly sensitive feature detection for high resolution LC/MS. BMC Bioinformatics *9*, 504.

55. Touw, W.G., Bayjanov, J.R., Overmars, L., Backus, L., Boekhorst, J., Wels, M., and van Hijum, S.A.F.T. (2013). Data mining in the Life Sciences with Random Forest: a walk in the park or lost in the jungle? Brief. Bioinformatics *14*, 315–326.

56. Hopkins, D.P., Cameron, D.D., and Butlin, R.K. (2017). The chemical signatures underlying host plant discrimination by aphids. Scientific Reports *7*, 8498.

57. Warnes, G.R., Bolker, B., Bonebakker, L., Gentleman, R., Huber, W., Liaw, A., Lumley, T., Maechler, M., Magnusson, A., and Moeller, S. (2009). gplots: Various R programming tools for plotting data. R package version *2*, 1.

58. Storey, J.D., and Tibshirani, R. (2003). Statistical significance for genomewide studies. PNAS *100*, 9440–9445.

59. Kaever, A., Lingner, T., Feussner, K., Göbel, C., Feussner, I., and Meinicke, P. (2009). MarVis: a tool for clustering and visualization of metabolic biomarkers. BMC Bioinformatics *10*, 92.

60. Kanehisa, M., and Goto, S. (2000). KEGG: kyoto encyclopedia of genes and genomes. Nucleic Acids Res. *28*, 27–30.

61. Kanehisa, M., Sato, Y., Furumichi, M., Morishima, K., and Tanabe, M. (2019). New approach for understanding genome variations in KEGG. Nucleic Acids Res. *47*, D590–D595.

62. Caspi, R., Billington, R., Fulcher, C.A., Keseler, I.M., Kothari, A., Krummenacker, M., Latendresse, M., Midford, P.E., Ong, Q., Ong, W.K., *et al*. (2018). The MetaCyc database of metabolic pathways and enzymes. Nucleic Acids Res *46*, D633–D639.

63. R Core Team (2018). R: A Language and Environment for Statistical Computing. Available at: https://www.R-project.org/.

64. Wickham, H. (2016). ggplot2: Elegant Graphics for Data Analysis.

65. Pinheiro, J., Bates, D., DebRoy, S., Sarkar, D., and R core Team (2019) (2019). nlme: Linear and Nonlinear Mixed Effects Models. Available at: https://CRAN.R-project.org/package=nlme.

KEY RESOURCES TABLE

REAGENT or RESOURCE	SOURCE	IDENTIFIER
Bacterial and Virus Strains		
Serratia marscesens	Collection of Institut Pasteur	CIP 103235T
Chemicals, Peptides, and Recombinant Proteins		
Protozoan Pellet Media	Carolina Biological Supply	132360
Paraquat dichloride	Sigma-Aldrich	36541; CAS: 75365-73-0
8-peak rainbow calibration particles	BioLegend	422903
Chelex100 resin	Bio-Rad Laboratories	1421253
Deposited Data		
Mass spectrometry data, fluorimetry data and flow cytometry data	This paper	DOI: 10.17632/6zspctmwpj.1
Experimental Models: Organisms/Strains		
P. bursaria – *Chlorella* 186b strain	Culture Collection of Algae and Protozoa	CCAP 1660/18
P. bursaria – *Chlorella* HA1 strain	National BioResource project	NBRP ID: PB034004A
Oligonucleotides		
ISSR primer '65': AGAGAGAGAGAGAGAGCC	Shen (2008)	N/A
Software and Algorithms		
ImageJ v1.50i	Schneider et al., 2012	https://imagej.nih.gov/ij/
xcms R package	Benton et al., 2010; Smith et al., 2006; Tanutenhahn et al., 2008	https://bioconductor.org/packages/release/bioc/html/xcms.html
MarVis-Suite 2.0 software	Kaever et al., 2009	http://marvis.gobics.de/

Figure 1

Click here to access/download;Figure;Figure 1.tif

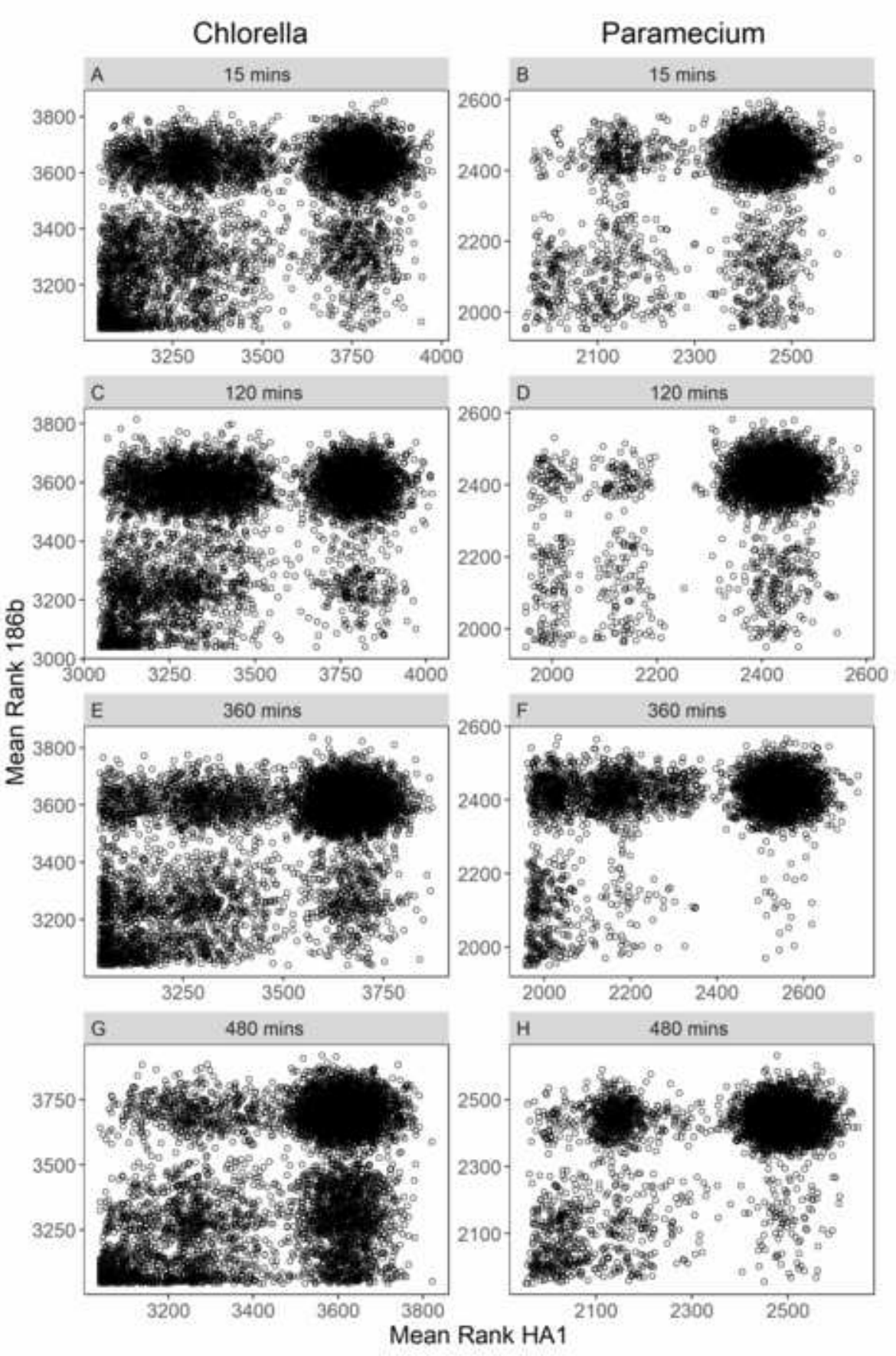

Figure 2

Click here to access/download;Figure;Figure 2.tif

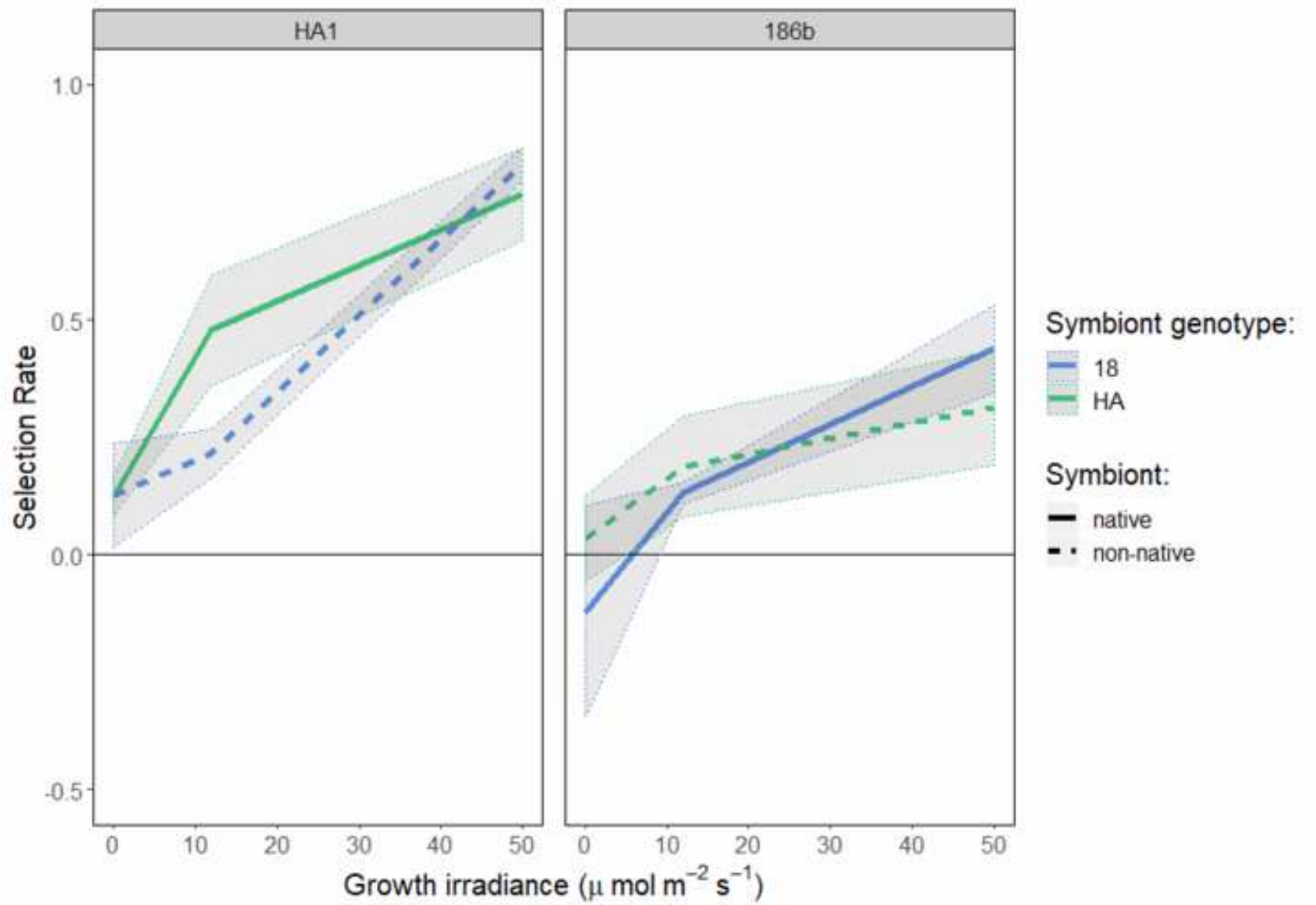

Figure 3

Click here to access/download;Figure;Figure 3.tif

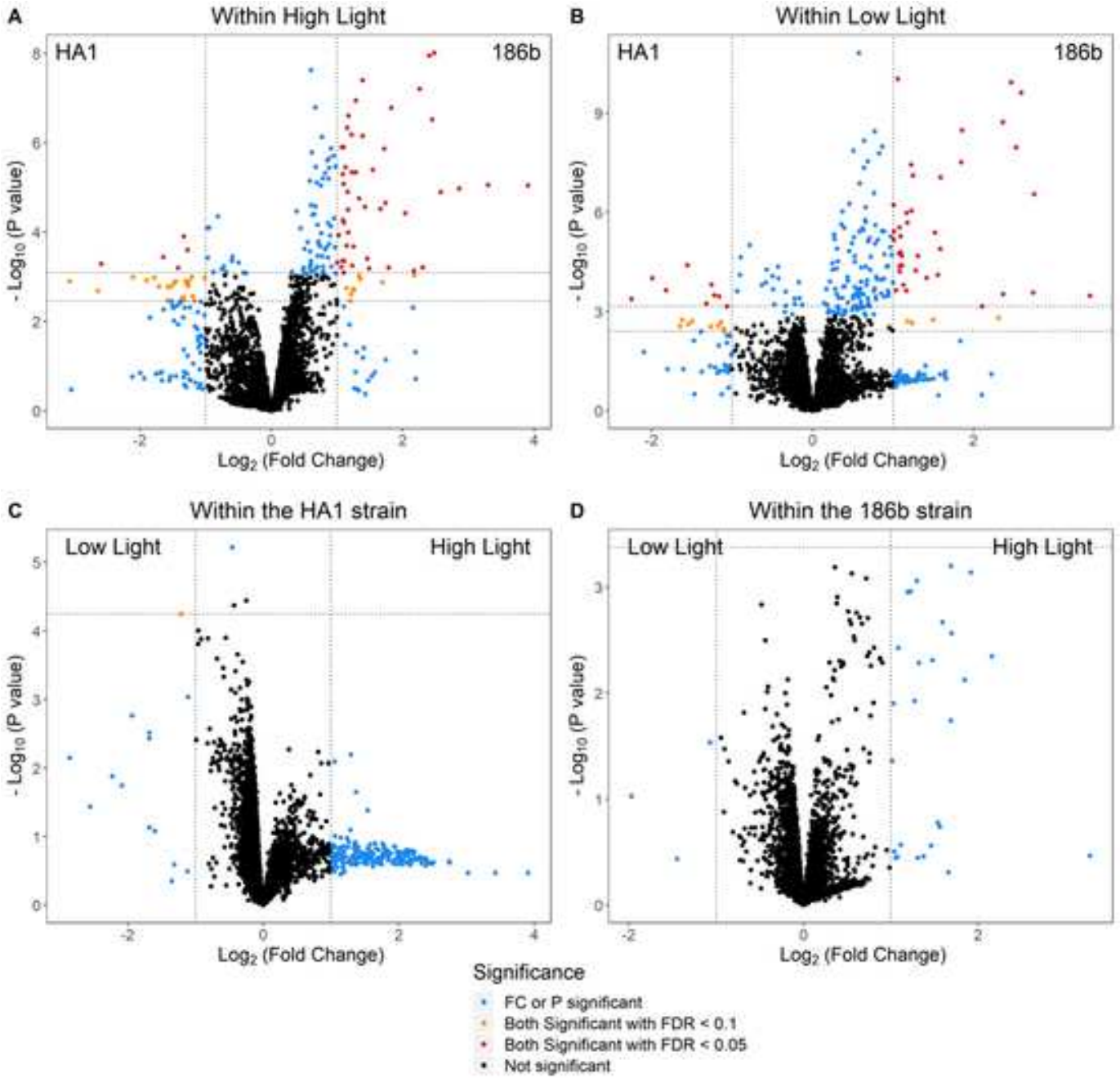

Figure 4

Click here to access/download;Figure;Figure 4.tif

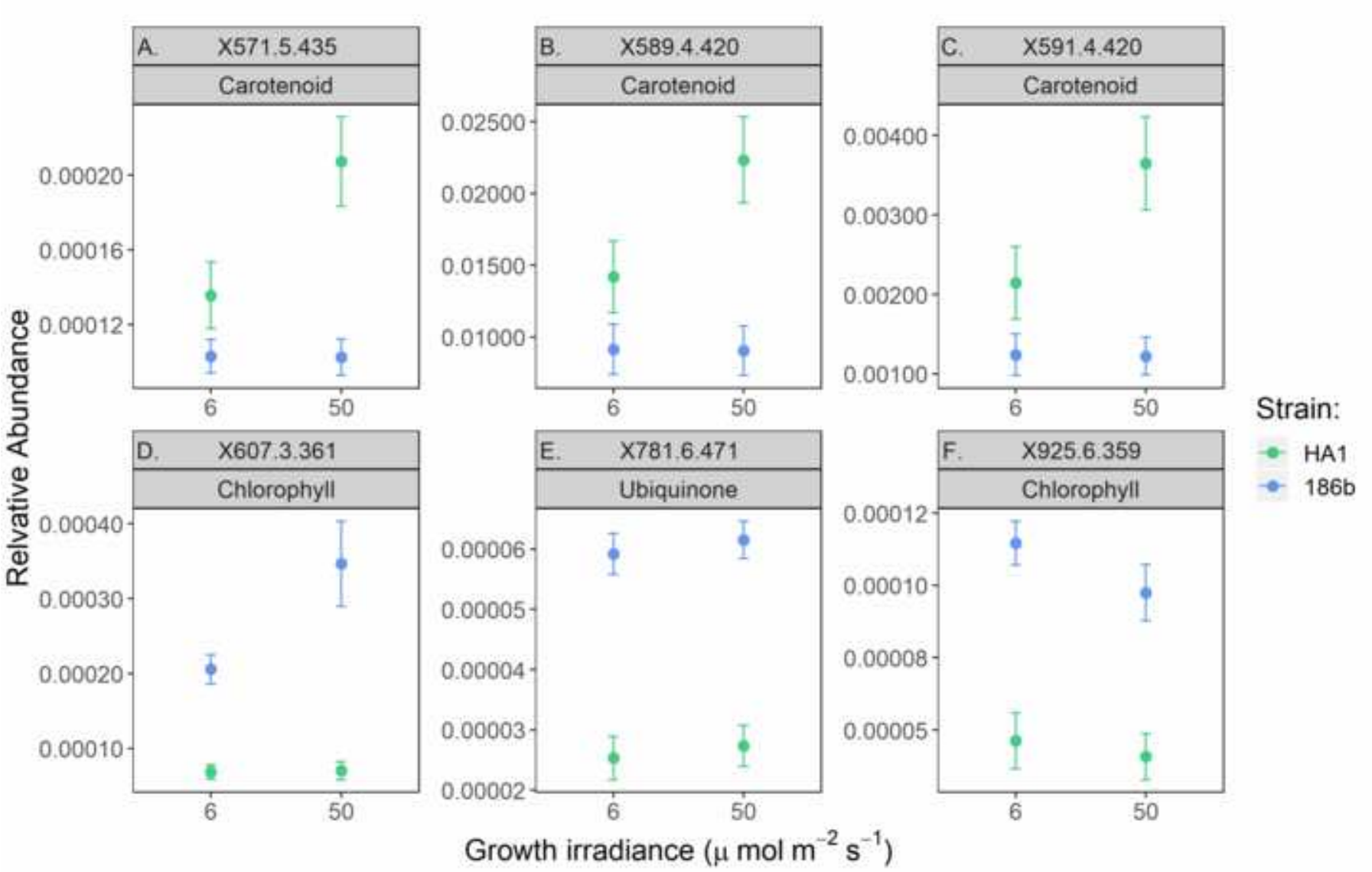

Figure 5

Click here to access/download;Figure;Figure 5.tif

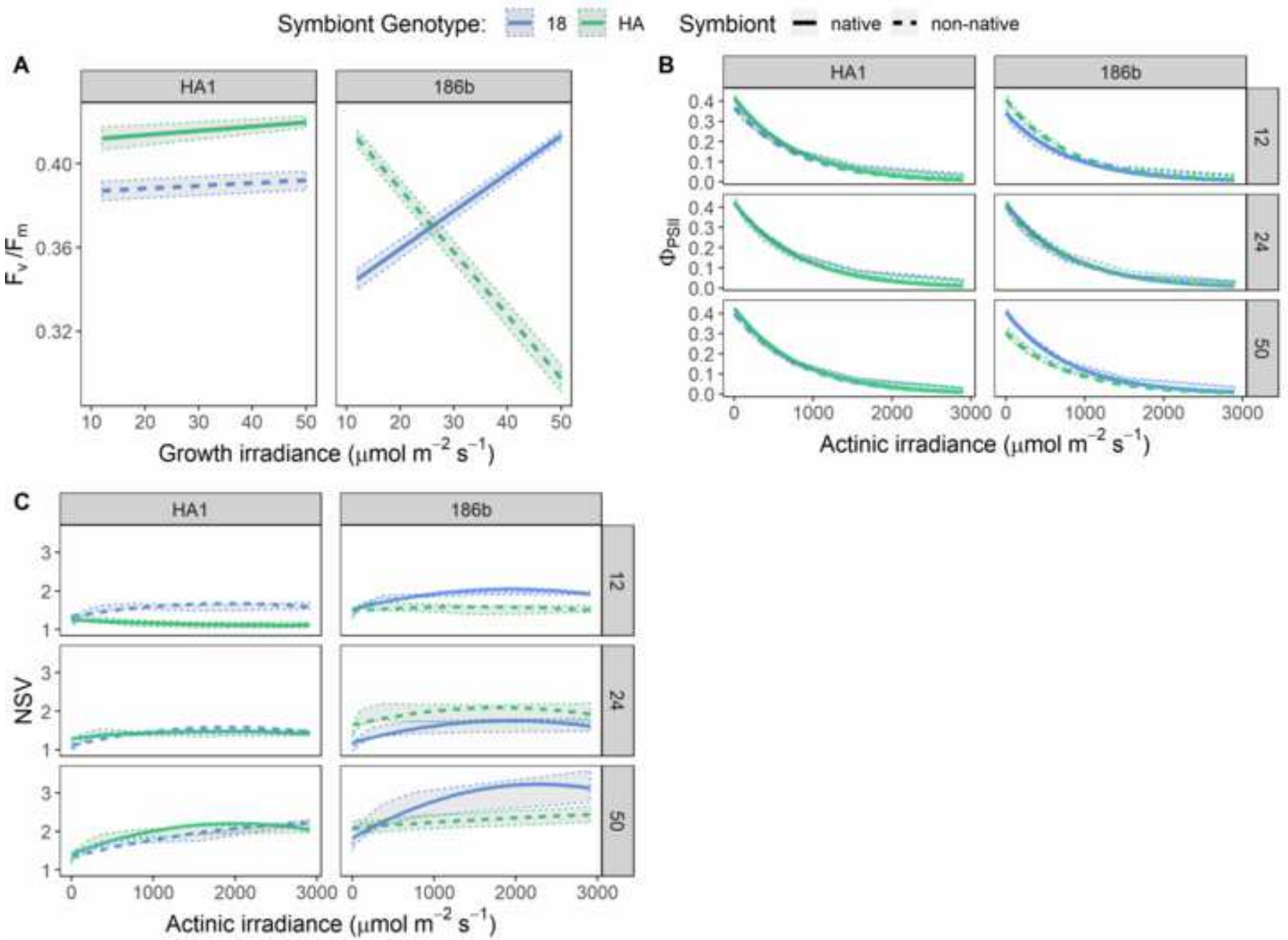

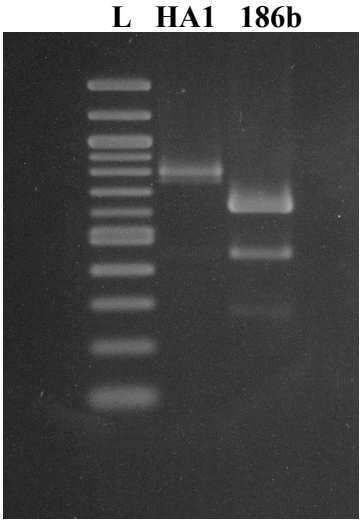

Figure S1: Diagnostic PCR between the HA1 and 186b *Chlorella* strains. **Related to main text.**

Showing clear banding pattern differences with the ’65 ISSR’ primer. Shown with a 100 bp ladder.

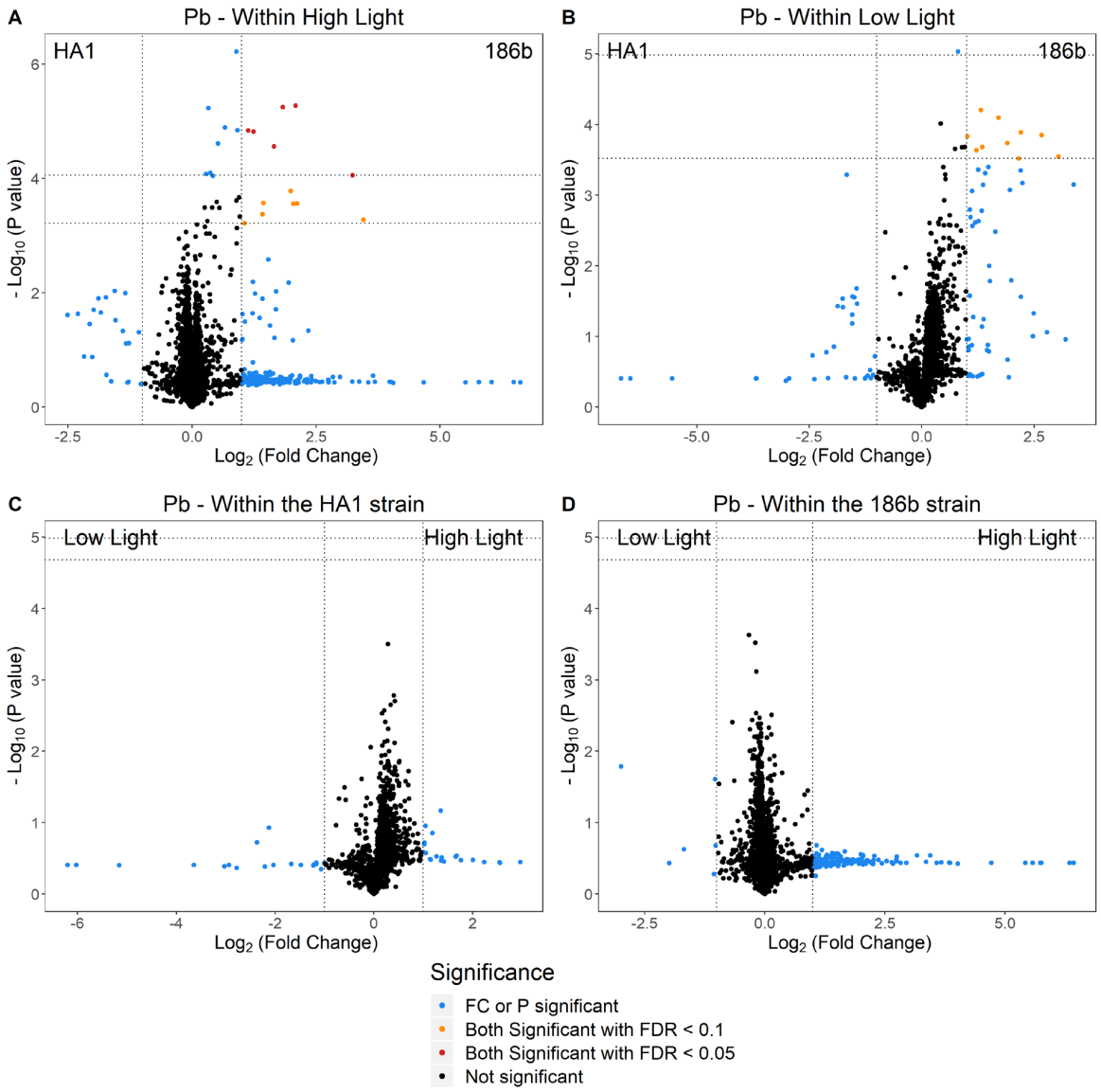

Figure S2: Comparisons of the unlabelled *Paramecium* metabolites between the strains and light conditions. Related to Figure 3.

Volcano plots for the unlabelled *Paramecium* metabolite comparisons. Plotting the fold change of each metabolite against its statistical significance. The data points are highlighted at two false discovery rate (FDR) values, and if the Log_2(fold change) is greater than 1 or less than -1. A.) Comparing the expression between the two strains within the high light condition. B.) Comparing the expression between the two strains within the low light condition. C.) Comparing expression between the two light levels within the HA1 strain. D.) Comparing expression between the two light levels within the 186b strain.

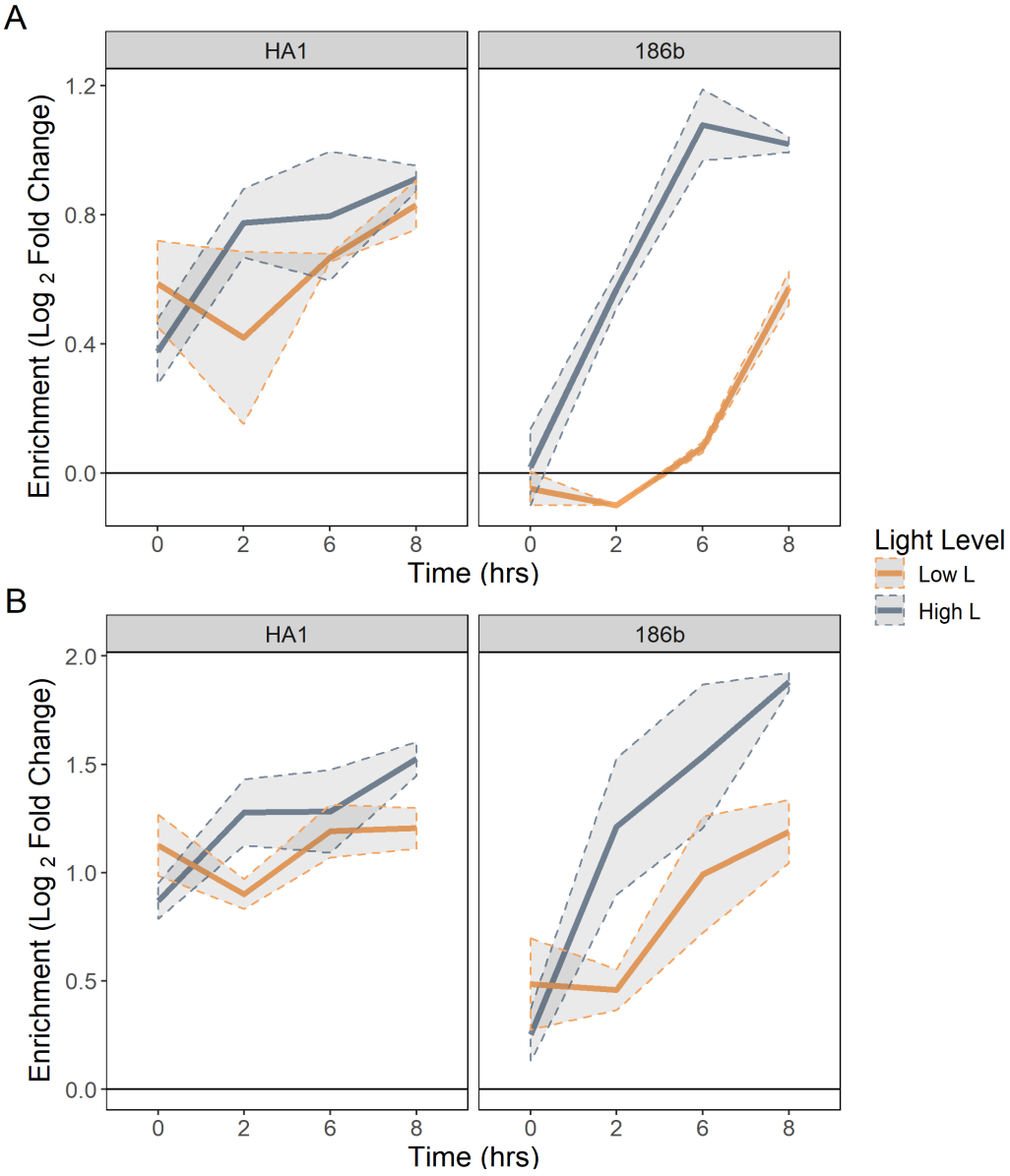

Figure S3: The interaction of light intensity and strain identity on the C^{13} enrichment profile of carbohydrate metabolites in the *Paramecium* fraction. Related to the main text.

For all panels, the enrichment value is the Log2 of the Fold Change in enrichment of the C^{13} labelled fraction compared to the control. Presented as the mean (n=3) ±SE. The low light level refers to 6 µmol m^{-2} s^{-1} and the high light to 50 µmol m^{-2} $s^{-}1$. A) Profile of 689.2 mz, 16 rt, Glycogen. B) Profile of 365.1 mz, 16 rt, a disaccharide, thought to be sucrose.

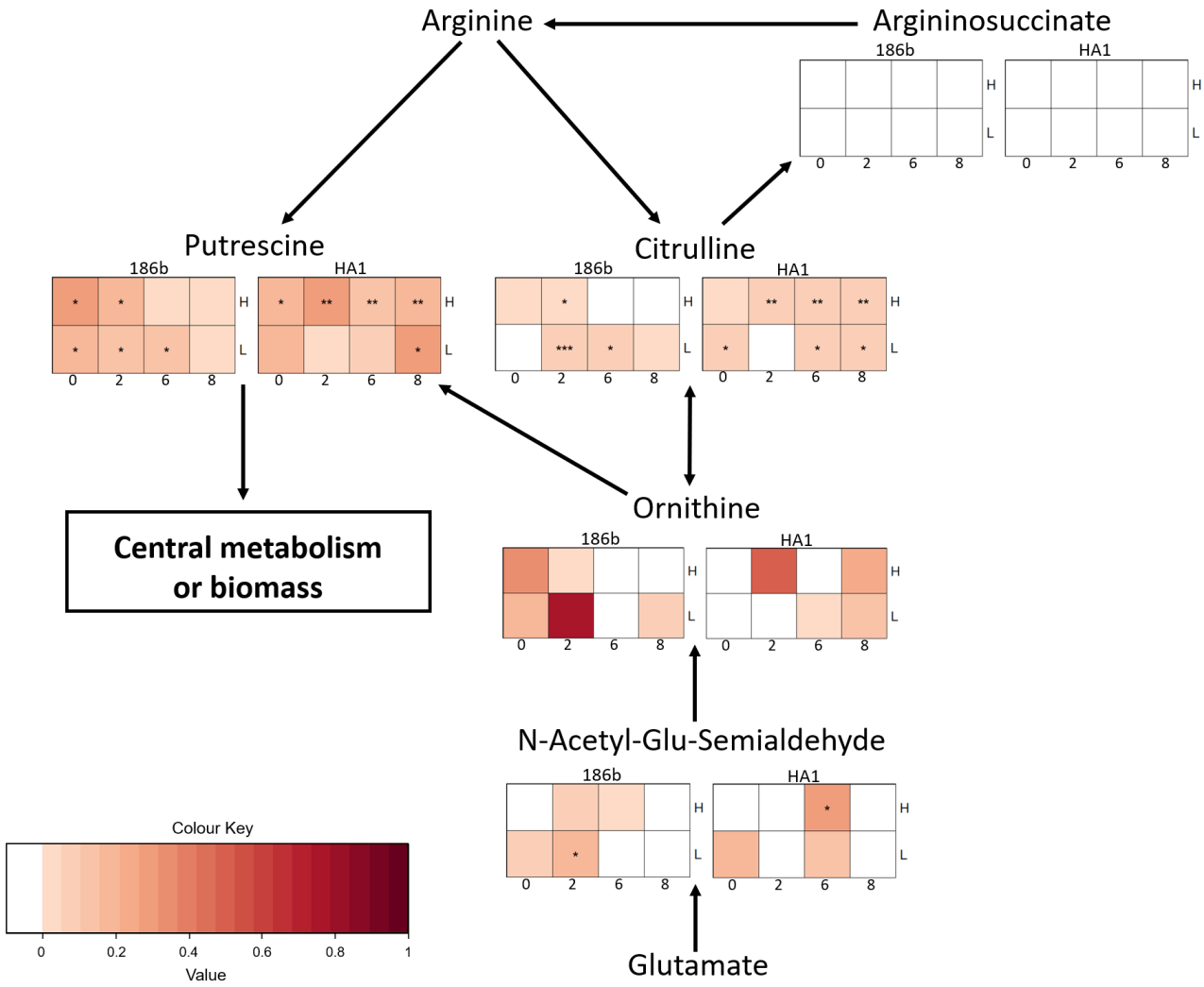

Figure S4: Schematic pathway diagram of nitrogen enrichment in the amino acid metabolism of the *Chlorella* metabolic fraction. Related to the main text and STAR methods.

The tables show relative N^{15} enrichment across time (in hrs), in the two light conditions (H = 50 µmol m^{-2} s^{-1}, L = 6 µmol m^{-2} s^{-1}). The colour corresponds to the fold change of the enrichment compared to the control, with significance stars indicating the statistical strength of this change. The nitrogen enrichment is focused downstream from arginine; ornithine, putrescine and citrulline possessed clear enrichment profiles while upstream compounds such as arginosuccinate had no detectable enrichment. This analysis is further explained in the STAR methods section.

Table S1. Details of the *P. bursaria* – *Chlorella* strains. Related to main text.

Strain	Year	Location	Latitude and Longitude	Elevation	Average Temperature Range	Average Total Sunshine hours a year	Culture Collection
186b	2006	Lilly Loch, Inverawe, Scotland, UK	56°26'03.8"N 5°12'22.1"W	20-40m	2.3°c to 17.9°c [1]	1,219.4 hrs [1]	CCAP 1660/18 [2]
HA1	2010	Hirosaki-city, Aomori pref, Japan	40°35'35.02"N 140°28'21"E	45m	-5°c to 28°c [3]	2013.2 hrs [3]	NBRP ID: PB034004A [4]

[1] Based on the Met Office UK Climate averages data for Dunstaffnage (https://www.metoffice.gov.uk/research/climate/maps-and-data/uk-climate-averages)

[2] https://www.ccap.ac.uk/strain_info.php?Strain_No=1660/18

[3] Based on data for Hirosaki city and Aomori airport (https://www.japanhoppers.com/en/tohoku/hirosaki/weather/) (https://www.worldweatheronline.com/hirosaki-weather-averages/aomori/jp.aspx)

[4] http://nbrpcms.nig.ac.jp/paramecium/wp-content/themes/paramecium/data/strain_ha1g.pdf

Table S2. List of metabolite IDs found to be co-enriched with N^{15} in the *Chlorella* fraction and their candidate identifications. Related to Figure 1.

RF Time	Detected Mass	Retention Time	Pathway	Candidate Compounds	Exact Mass	Adduct	KEGG/ MetaCyc
1	113	482	Pyrimidine/Amino acid	Uracil	112.0273	H+	C00106
				1,3-diaminopropane	74.0844	K+	C00986
1	166	478	Purine	5-Amino-4-imidazole carboxylate	127.0382	K+	C05516
1,2	237.1	286	Biotin	Dethiobiotin	214.1317	Na+	C01909
1,2,3,4	871.6	405	Chlorophyll	Pheophytin A	870.5659	H+	C05797
1,2,4	593.3	405	Chlorophyll	Pheophorbide A	592.2686	H+	C18021
				Urobilinogen	592.3261	H+	C05790
2,3	140	213	Amino acid	L-Aspartate 4-semialdehyde	117.0426	Na+	C00441
				Indole	117.0578	Na+	C00463
				1-Aminocyclopropane-carboxylate	101.0477	K+	C01234
				5-Aminopentanal	101.0841	K+	C12455
3	482.4	324	Folate biosynthesis	Dihydrofolate	443.1553	K+	C00415
3	848.6	294	Ubiquinone	Rhodoquinone-10	847.6842	H+	CPD-9613
4	227.1	460	Amino acid/Chlorophyll	Tryptophan	204.0899	Na+	C00078
				Porphobilinogen	226.0954	H+	C00931

Table S3. List of metabolite IDs found to be co-enriched with C^{13} in the *P. bursaria* fraction and their candidate identifications. Related to Figure 1.

RF Time	Detected Mass	Retention Time	Pathway	Candidate Compounds	Exact Mass	Adduct	KEGG
1	100	16	Glycerophospholipid	Ethanolamine	61.0528	K+	C00189
1	689.2	16	Carbohydrate	Glycogen	666.2219	Na+	C00182
1,2	124	15	Vitamins and Cofactors	Niacin	123.032	H+	C00253
1,2	261	14	Carbohydrate	Monosaccharide phosphate	260.0297	H+	C00092
1,2,3	251	17	Isoprenoid pathway	(R)-5-Phosphomevalonate	228.0399	Na+	C01107
1,2,3,4	190	341	Phosphonate	Demethylphosphinothricin	167.0347	Na+	C17962
1,2,3,4	441.3	310	Lipid	Hydroxycholesterol	402.3498	K+	C05500
1,2,3,4	639.2	414	Heme biosynthesis	Haem	616.1773	Na+	C00032
1,2,3,4	212.9	479	Chlorocyclohexane and chlorobenzene degradation	Chlorodienelactone	173.972	Ka+	C04706
1,2,4	109	479	Quinone	p-Benzoquinone	108.0211	H+	C00472
1,2,4	345.9	480	Amino acid metab	3-Iodo-L-tyrosine	306.9705	K+	C02515
1,3,4	169	19	Central metabolism	2-Oxoglutarate	146.0215	Na+	C00026
				2-Oxoisocaproate	130.063	K+	C00233
				3-Methyl-2-oxopentanoate	130.063	K+	C00671
				2-Dehydropantoate	146.0579	K+	C00966
				3-Phosphonopyruvate	167.9824	H+	C02798
				Phosphoenolpyruvate	167.9824	H+	C00074
2	313.2	287	Lipid	HPODE	312.2301	H+	C04717
2,3,4	519.1	400	Peptide	Nitro-hydroxy-glutathionyl-dihydronaphthalene	496.1264	Na+	C14803
2,4	71.1	373	Amino acid	Aminopropiononitrile	70.0531	H+	C05670
3	405.1	236	Isoprenoid pathway	Farnesyl diphosphate	382.131	Na+	C00448

Table S4. The metabolite IDs and candidate identification for the metabolites of interest from the unlabelled metabolic analyses. Related to Figure 3 and S2.
These metabolites were therefore upregulated in either one of the strains or in one of the light conditions. This table includes both the *Chlorella* and *P. bursaria* results.

Fraction	Upregulated in	Condition	Detected Mass	Retention Time	FDR	Pathway	Candidate Compounds	Exact Mass	Adduct	Kegg / Metacyc
Chlorella	**HA1 strain**	**H & L light**	247.2	336	*,**	Alkaloid/quinone	Anapheline	224.1889	Na+	C06183
							Geranylhydroquinone	246.162	H+	C10793
			283.3	336	*,**	Fatty acid	Oleate	282.2559	H+	C00712
		H light	218.2	17	*	Amino acid	L-Glutamylputrescine	217.1426	H+	C15699
							Alanyl-L-lysine	217.1426	H+	C05341
			265.3	337	*	Fatty acid	1-Hexadecanol	242.261	Na+	C00823
			385.2	375	*	Plant Hormone	Gibberellin A36	362.1729	Na+	C11862
			571.5	435	*	Carotenoid	Methoxyneurosporene	570.4801	H+	C15895
			589.4	420	*	Carotenoid	Echinenone	550.4175	K+	C08592
							Anhydrorhodovibrin	566.4488	Na+	C15877
							Hydroxychlorobactene	550.4175	K+	C15911
							3-Hydroxyechinenone	566.4124	Na+	C15966
			591.4	420	*	Carotenoid	Zeaxanthin	568.428	Na+	C06098
							Zeinoxanthin	552.4331	K+	C08590
							beta-Cryptoxanthin	552.4331	K+	C08591
							Xanthophyll	568.428	Na+	C08601
	Low Light	**HA1 strain**	743.5	373	*	Phosphoglyceride	1-18:3-2-trans-16:1-phosphatidylglycerol	742.4785	H+	CPD-2186
	186 Strain	**H & L light**	105	15	*,**	Central metabolism	Hydroxypyruvate	104.011	H+	C00168
							Allophanate	104.0222	H+	C01010
			169	17	**	Central metabolism	2-Oxoglutarate	146.0215	Na+	C00026
							Phosphoenolpyruvate	167.9824	H+	C00074
							3-Phosphonopyruvate	167.9824	H+	C02798
							2-Oxoisocaproate	130.063	K+	C00233
							3-Methyl-2-oxopentanate	130.063	K+	C00671
							2-Dehydropantoate	146.0579	Na+	C00966
							Coumarin	146.0368	Na+	C05851
			273.2	395	**	Fatty Acid	16-Hydroxypalmitate	272.2351	H+	C18218
			289.3	244	**	Diterpenoid	Kaurenol	288.2453	H+	C11872

Table S4 continued

Fraction	Upregulated in	Condition	Detected Mass	Retention time	FDR	Pathway	Candidate Compounds	Exact mass	Adduct	KEGG
Chlorella			337.3	380	**	Fatty acids	13;16-Docosadienoic acid	336.3028	H+	C16533
			607.3	361	**	Chlorophyll	Protoporphyrinogen IX	568.305	K+	C01079
			781.6	471	**	Ubiquinone	3-methoxy-4-hydroxy-5-nonaprenylbenzoate	780.2	H+	CPD-9898
			925.6	359	**	Chlorophyll	Bacterio-pheophytins	888.5765	K+	C05798
		H light	262.1	248	**	Folate	Dihydrobiopterin	239.1018	Na+	C00268
							6-Lactoyl-5;6;7;8-tetrahydropterin	239.1018	Na+	C04244
			323.2	248	*	Photoreception	Vitamin A aldehyde	284.214	K+	C00376
			335.3	372	**	Isoprenoids	Phytol	296.3079	K+	C01389
			751.5	366	**	Ubiquinone	Octaprenyl-methyl-hydroxy-methoxy-1;4-benzoquinone	712.5431	K+	C05815
		L light	273.3	268	**	Diterpenoid	Ent-Kaurene	272.2504	H+	C06090
P. bursaria	**186 strain**	**H & L light**	124	238	**, *	Vitamins and Cofactors	Niacin	123.032	H+	C00253
			126	217	**, *	Sulfur metabolism	Taurine	125.0147	H+	C00245
			170	237	**, *	Amino acid	Glutamate	147.0532	Na+	C00025
							5-Amino-4-oxopentanoate	131.0582	K+	C00430
							Glutamate 5-semialdehyde	131.0582	K+	C01165
			364.2	236	*, *	Antibiotic ?	ACV	363.1464	H+	C05556
			396.1	237	*,*	Antibiotic ?	Deacetylcephalosporin C	373.0944	Na+	C03112
							Novobiocic acid	395.1369	H+	C12474
		H light	352.2	237	*	Plant hormone?	trans-Zeatin riboside	351.1543	H+	C16431
			390.1	237	*	Amino/nucleotide sugar	N-Acetylneuraminate 9-phosphate	389.0723	H+	C06241
			416.1	250	**	Antibiotic ?	Cephalosporin C	415.1049	H+	C00916
							Chlorobiocic acid	415.0823	H+	C12471
			434.1	249	*	Antibiotic ?	Novobiocic acid	395.1369	K+	C12474
		L light	418.2	268	*	Sphingolipid	Sphingosine 1-phosphate	379.2488	K+	C06124